Optics Communications 335 (2015) 23–27

Contents lists available at ScienceDirect

Optics Communications

journal homepage: www.elsevier.com/locate/optcom

Role of the immersion medium in the microscale spherical lens imaging

Ling Yao [a], Yong-Hong Ye [a,*], Hui Feng Ma [b], Lingling Cao [a], Jinglei Hou [a]

[a] *Jiangsu Provincial Key Laboratory of Optoelectronic Technology, Department of Physics, Nanjing Normal University, Nanjing 210097, China*
[b] *State Key Laboratory of Millimeter Waves, Southeast University, Nanjing 210096, China*

ARTICLE INFO

Article history:
Received 27 June 2014
Received in revised form
15 August 2014
Accepted 22 August 2014
Available online 6 September 2014

Keywords:
Immersion medium
Microsphere
Fourier components

ABSTRACT

The role of the immersion medium in the microscale speherical lens imaging is studied. We find that when a microsphere lens is semi-immersed in the SU-8 resist, both the microsphere and the SU-8 resist can work as a lens. The microsphere lens forms the images from the small-k Fourier components of an object, and this image formation does not depend on the immersion of the SU-8 resist. The SU-8 resist can work as a lens and form the images from the large-k Fourier components. When the distance d between the focal spot of the SU-8 lens and the object is close, the clear large-k Fourier components image can be observed even without the microsphere.

1. Introduction

In geometrical optics, a lens-based optical microscope cannot resolve features of an object small than $\lambda/2$ (λ, wavelength) in the far-field due to Abbe's diffraction limit. Recently, it has been found that microscale and nanoscale lenses can magnify and resolve features beyond the diffraction limit [1–17]. Lee et al. [7] have reported near-field high resolution by nanoscale spherical lenses. Wang et al. [10] have reported optical virtual imaging at 50 nm lateral resolution with a white-light nanoscope. Hao et al. [12] have shown that the magnified virtual image has a sharper contrast when the microscale spherical lens is semi-immersed in liquid. Darafsheh et al. [14] have been experimentally shown optical super-resolution imaging by high-index liquid-immersed microspheres. Li et al. [15] have described direct white-light optical imaging of 75-nm adenoviruses by submerged microsphere optical nanoscope. Among these studies, the microsphere lenses are immersed or semi-immersed in a medium in many cases. Compared to the well-studied solid immersion microscale lenses, the role of the immersion medium in the microscale lens imaging remains to be further revealed [18–20]. Our recent experimental results reveal that when a microsphere lens is semi-immersed in a medium, it can intercept more large-k Fourier components of the object, and it has two image channels [21]. However, it has not been answered whether the immersion medium involves in the image formation or just helps to increase the contrast of the image. In this paper, we study the role of the immersion medium (SU-8 resist) in the microsphere lens imaging. We find that the immersion medium can work as a microscale lens. When the microsphere lens is removed, leaving the air hole semi-immersed in the SU-8 resist, it might still form the image of the large-k Fourier components of the object. Our findings will advance the understanding of the super-resolution imaging mechanisms in microscale lenses.

2. Experimental

Three types of samples are fabricated, as shown in Fig. 1(a). The detailed fabrication process can be found in one of our previous publications [21]. Two kinds of polystyrene (PS) microspheres, with a diameter of 280 or 710 nm, are used as objects in the experiments. Fig. 1(b) illustrates the schematic of the experimental setup. The samples were put under a Leica microscope (DM 2500 M), and the reflected images of the PS microsphere arrays through the 4.87-μm-diameter silica microsphere lens (types A and B samples), or the 4.87-μm-diameter air hole immersed in the SU-8 resist (type C samples) were recorded by a 100 × (NA = 0.9) microscope objective with a charge-coupled device camera. The light source in the microscope is a halogen lamp. During the experiments, the position of the microscope objective was moved in order to focus the formed images. The schematic positions of both the virtual image plane and the real image plane are also indicated in Fig. 1(b). Fig. 1(c) is the scanning electron microscope (SEM, Hitachi S-48000) image of a typical self-assembled PS microsphere array. Optical microscope images of the PS microsphere array are also gave (Supplementary Fig. S1).

---

* Correponding author.
E-mail address: yenjnu@yahoo.ca (Y.-H. Ye).

http://dx.doi.org/10.1016/j.optcom.2014.08.051
0030-4018/

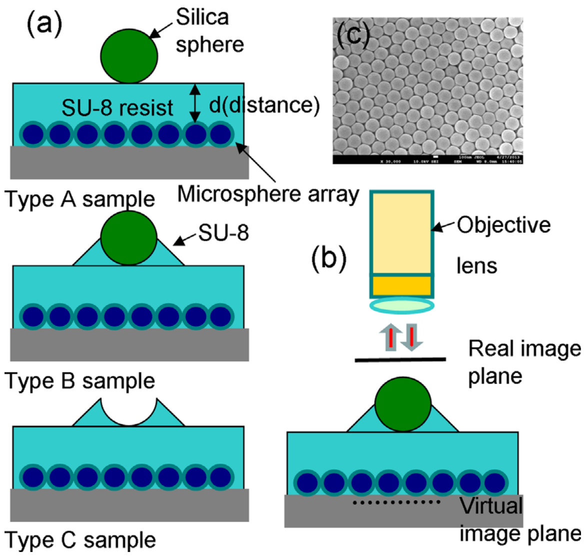

Fig. 1. (a) Schematic of the three types of samples; (b) schematic of the experimental setup; (c) SEM image of a self-assembled PS microsphere array. The diameter of the PS microspheres is 710 nm in this sample.

3. Results and discussion

Fig. 2 is the optical microscope images of the large object (the 710 nm PS microspheres) at $d=2.9$ µm (d is the distance between the object and the 4.87-µm-diameter silica microsphere lens), and the optical images of the microsphere lens (or the 4.87-µm-diameter air hole immersed in the SU-8 resist) are also shown in the figure. As shown in Fig. 2(a), a blurred real image (a-2) is observed in the type A sample, and its magnification factor M is about $-1.31\times$. a-1 is the optical image of the microsphere lens. As illustrated in Fig. 2(b), both a real image (b-2) and a virtual image (b-3) are formed in the type B sample. The virtual image is sharper and clear, with a M of $1.52\times$; the real image is blurring, with a M of $-1.5\times$. b-1 is the optical image of the microsphere lens, and this lens is bigger than the one in Fig. 2(a) due to the semi-immersion of the SU-8 resist. As shown in Fig. 2(c), the microsphere is removed, leaving the air hole semi-immersed in the SU-8 resist (c-1) in the type C sample. However, one clear and sharper virtual image (c-2, $M=1.49\times$) can be found. Fig. 2(d) is the SEM images of the side (d-1) and top views (d-2) of the type C sample. Fig. 2(d) clearly shows that the microsphere lens is removed, leaving the air hole semi-immersed in the SU-8 resist. Moreover, the PS microsphere object under the air hole (the object) is kept.

Fig. 3 shows the optical microscope images of the small object (the 280 nm PS microspheres) at $d=2.9$ µm. For the type A sample, no obvious images can be observed (Fig. 3(a)). For the type B sample, a clear virtual image is formed (Fig. 3(b), $M=1.5\times$). As indicated in Fig. 3(c), the clear virtual image still exists, and M is about $1.51\times$ in the type C sample. The imaging properties of both the small and large objects at $d=5.4$ µm are also studied (Supplementary Fig. S2 and S3). The imaging behaviors are similar at the two distances (2.9 and 5.4 µm).

Moreover, the optical microscope images of the large object samples at $d=0$ µm are also studied. As shown in Fig. 4, for the types A and B samples, their imaging behaviors are similar to the case when d is 2.9 or 5.4 µm. As shown in Fig. 4(a), for the type A sample, a virtual image is formed and M is around $2.7\times$. A blurring virtual image (b-1, $M=2.68\times$) and a clear virtual image (b-2, $M=1.57\times$) are observed in the type B sample. However, Fig. 4(c) reveals that no images are observed in the type C sample, which is different from the case when d is 2.9 or 5.4 µm.

Fig. 5 displays the optical microscope images of the small object samples at $d=0$ µm. No images can be observed for the types A (Fig. 5(a)) and C (Fig. 5(c)) samples. A clear virtual image is found for the type B sample (Fig. 5(b), $M=1.68\times$). Moreover, the imaging properties of both the small and large objects at $d=1.5$ µm are also studied. The behaviors are similar at the two distances (0 and 1.5 µm).

Fig. 6 shows the optical microscope images of the large object at $d=12$ µm. Fig. 6(a) reveals that no images are observed for the type A sample. Only a clear virtual image (Fig. 6(b), $M=1.10\times$) is found for the type sample B. As indicated in Fig. 3(c), the clear virtual image ($M=1.05\times$) still exists in the type C sample. We also studied the imaging properties of the small object at $d=12$ µm, but we cannot observe any images for the three types of samples.

Objects contain information at many different spatial scales, from fine (large-k Fourier components) to coarse (small-k Fourier components). The insets in Figs. 2–6 are the frequency spectra of the images which are calculated by the 2D Fourier transform. The white dots in the insets represent the high amplitude of Fourier transform of the images, while the dark dots represent the low amplitude. The low frequencies are located at the center of the insets, while the high frequencies are located at the corners. The frequency spectra show that the blurred images mainly have small-k Fourier components, while the clear images have more large-k components than the blurred images have. Therefore, The blurring images in Figs. 2–5 are the small-k Fourier components of the large objects, while the clear and sharper images in Figs. 2–6 are the large-k Fourier components of the objects. When a SU-8 layer is coated on top of the objects, the Rayleigh resolution limit for point objects is 229 nm ($r=0.61\ \lambda/n\mathrm{NA}$), here $\lambda=540$ nm, $n=1.6$ (the refractive index of SU-8), and NA$=0.9$ [22]. Therefore, the small objects (280 nm microspheres), are close to the resolution limit. Our experimental results indicate that: (1) the microsphere lens and d play major roles in the formation of the blurred image (small-k Fourier components of the object). If the microsphere lens is dissolved or the d is too long, no blurred images can be observed; (2) the semi-immersion medium (SU-8 resist) plays an important role in the clear image (large-k Fourier components) formation. The SU-8 resist can work as a lens, forming the clear super resolution images. At $d=2.9$, 5.4, and 12 µm, even the microsphere is removed, the clear images can still be formed. As long as the microsphere lens is semi-immersed in the SU-8 resist, the clear images can always be observed; (3) for types B and C samples, the magnification factor M of the clear virtual images decreases as the distance d increases. At $d=12$ µm, because of the small magnification of the clear virtual images, the clear virtual images of the small object cannot be observed.

To find out the mechanisms in the image formation, finite-difference time-domain (FDTD) simulations were carried out using CST program. CST is a commercial FDTD program by calculating the exact solution of Maxwell's equation. Fig. 7 is the simulated focusing properties of the three types of microscale lens systems related to the three types of samples. Fig. 7(a) shows that there is only one focal spot (F is ~0.7 µm) for the microsphere lens. When the microsphere lens is semi-immersed in the SU-8 resist, there are two focal spots. One is at 0.7 µm, while the other is at about 10.1 µm, as shown in Fig. 7(b). For the air hole semi-immersed in the SU-8 resist system, there is one focal spot with $F=10.1$ µm. The full width half at maximum (FWHM) of the focal spots in Fig. 7(b) and Fig. 7(c) is wider than the FWHM of the focal spot in Fig. 7(a) (Supplementary Fig. S4). The simulated results indicate that both the microsphere lens and the immersion SU-8 resist can work as a lens separately. The microsphere lens forms the images from the small-k Fourier components. Therefore, when the microsphere lens is removed, no blurred images can be formed, as shown in Figs. 2–5. The semi-immersion of the SU-8 resist cannot only intercept more large-k Fourier components, but can work as a lens